



# Faster Taylor bubbles

Guangzhao Zhou<sup>1</sup> and Andrea Prosperetti<sup>1,2,3,†</sup>

<sup>1</sup>Department of Mechanical Engineering, University of Houston, Houston, TX 77204, USA

<sup>2</sup>Faculty of Science and Technology, University of Twente, 7500 AE, Enschede, The Netherlands

<sup>3</sup>Department of Mechanical Engineering, Johns Hopkins University, Baltimore, MD 21218, USA

(Received 25 March 2021; revised 22 April 2021; accepted 12 May 2021)

Gas volumes with an equivalent spherical diameter greater than that of the tube in which they rise by buoyancy – so-called Taylor bubbles – assume a characteristic bullet shape and ascend with a velocity that is dependent primarily on the tube diameter, and also on the physical properties of the liquid, but, remarkably, is mostly independent of the gas volume. The requirement of liquid volume conservation suggests a plausible explanation of this paradoxical feature in that the space vacated under the rising bubble must be replenished by the liquid film falling along the bubble surface. It is demonstrated by numerical means that, by limiting the bubble diameter, a cylindrical ‘cage’ of thin vertical rods coaxial with the tube permits the flow rate of this film to increase, with the result that the bubble is able to ascend with a significantly higher velocity than in an empty tube with the same diameter.

**Key words:** gas/liquid flow, bubble dynamics, core–annular flow

## 1. Introduction

A paradoxical feature of large gas volumes rising in tubes – known as Taylor bubbles, after the work of Davies & Taylor (1950) – is that, when their length exceeds a few tube diameters  $D$ , their velocity of rise  $U_B$  becomes independent of length and depends only on  $D$  and the fluid properties. For large Reynolds numbers, for example, one has the relation  $U_B = K\sqrt{gD}$ , with  $g$  the acceleration of gravity and  $K \simeq 0.351$  a numerical constant (see e.g. Dumitrescu 1943; Bendiksen 1985; Fabre & Liné 1992). The precise mechanism underlying this result remains unclear, in spite of a large literature on the subject motivated by many applications in the oil, nuclear, chemical and other industries (see e.g. Fernandes, Semiat & Dukler 1983; Kulkarni & Joshi 2005; Lizarraga-Garcia *et al.* 2017; Zhang *et al.* 2018; Magnini *et al.* 2019), as well as in certain types of volcanic eruptions (see e.g. Gonnermann & Manga 2007; del Bello *et al.* 2012; Kawaguchi & Nishimura 2015). Commenting on a broadly applicable correlation for the rise velocity in

† Email address for correspondence: [aprosp@central.uh.edu](mailto:aprosp@central.uh.edu)

© The Author(s), 2021. Published by Cambridge University Press. This is an Open Access article, distributed under the terms of the Creative Commons Attribution licence (<https://creativecommons.org/licenses/by/4.0/>), which permits unrestricted re-use, distribution, and reproduction in any medium, provided the original work is properly cited.

dependence of various dimensionless parameters presented in Viana *et al.* (2003), Funada *et al.* (2005) observe, ‘One might say that the problem of the rise velocity has been solved without understanding.’

A perceptive remark in Funada *et al.* (2005) concerns the role of the ‘drainage’ caused by the liquid film falling in the gap between the bubble surface and the tube wall, which is evidently necessary to keep the space vacated by the rising bubble full of liquid. The authors observe, ‘A very convincing set of experiments showing the effect of drainage is reported . . . by Bi & Zhao (2001). They showed that for triangular and rectangular channels, elongated bubbles always rose upward even though the hydraulic diameter of the tube was as small as 0.866 mm, whereas in circular tubes the bubble motion stopped when  $d \leq 2.9$  mm. They did not offer an explanation but the reason is that surface tension cannot close the sharp corners where drainage can occur.’ Indirect support of this explanation can be found in the paper by Clanet, Héraud & Searby (2004), who correlated the rise velocity of Taylor bubbles in polygonal ducts in the form  $U_B = k\sqrt{gP}$ , in which  $P$  is the perimeter of the tube (which highlights the role of the drainage volumetric flow rate, which, for a fixed film thickness, increases with the perimeter of the tube cross-section) and  $k$  is a dimensionless constant.

These observations put a crucial focus on what must be the limiting factor determining the rise velocity of a Taylor bubble, namely the need for sufficient drainage flow along the tube wall to replenish the space vacated by the rising bubble. Since the pressure on the gas side of the falling film is essentially constant, the volumetric flow of this drainage is purely the result of a dynamic equilibrium between gravity and the no-slip condition at the tube wall, and is therefore independent of the bubble length. This is only a partial explanation of the paradox, though, because no proper theory is available for the film thickness beyond the very-low-Reynolds-number regime (Bretherton 1961). The literature contains several correlations (see e.g. Wallis 1969; Barnea 1990; Liberzon, Shemer & Barnea 2006; Nogueira *et al.* 2006; Llewellyn *et al.* 2012), but these are at best physically informed data fits and not the result of a full understanding of the problem.

Be that as it may, this explanation suggests that any arrangement able to increase the film drainage would be expected to increase the rise velocity of the Taylor bubble. It is the purpose of the present paper to describe such an arrangement which, indeed, produces the expected result.

## 2. Faster Taylor bubbles

We artificially increase the distance between the tube wall and the lateral surface of the bubble by constructing a ‘cage’ with an array of thin vertical rods regularly arranged on a circle coaxial with the tube as shown in figure 1. With a suitable spacing of the rods, surface tension is able to contain the gas within the core of the tube bounded by the cage. The wider annular space thus created facilitates the downward flow of liquid, and the bubble rise velocity is correspondingly increased, as can be seen in figure 2, in which the horizontal dashed line is the dimensionless bubble rise velocity in an empty tube (i.e. without the rod cage) according to the correlation of Viana *et al.* (2003). For all the cases simulated, the rise velocity of the bubble is larger than that in the empty tube, except for cases *K* and *L*, which are for the somewhat different arrangement shown in figure 9(b) and are addressed later in § 4.

The quantity shown in figure 2 is the Froude number, defined by

$$Fr = \frac{U_B}{\sqrt{gD}}. \quad (2.1)$$

### Faster Taylor bubbles

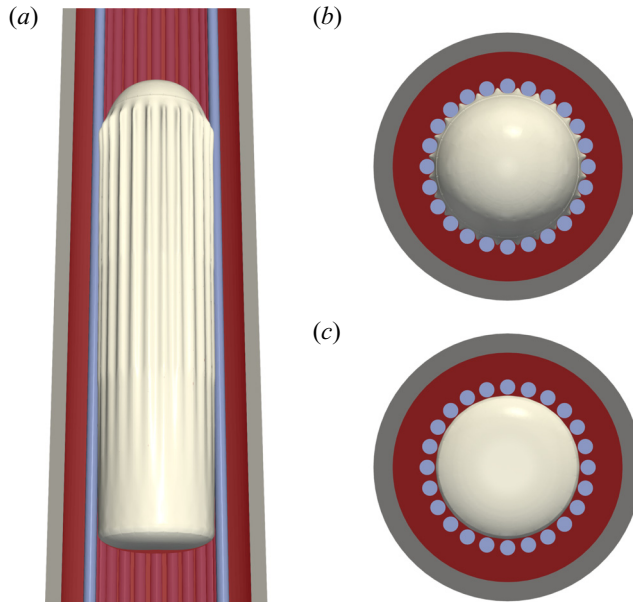


Figure 1. (a) The Taylor bubble rises inside a ‘cage’ of thin vertical rods (blue) arranged on a circle concentric with the tube axis. The images on the right are views of the rising bubble from above, (b), and from below, (c). The gas protrudes between the rods at the top, but as the pressure in the annulus increases downward, the bottom of the bubble becomes circular.

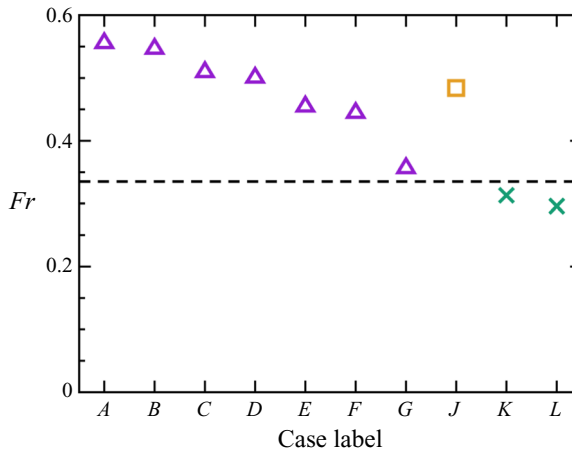


Figure 2. Dimensionless bubble rise velocity, or Froude number (2.1), for some of the cases presented in this paper. The pertinent parameters for each case are given in table 1. The horizontal dashed line is the value predicted by the correlation of Viana *et al.* (2003) for the parameters of case A.

The parameters characterizing each simulation are given in table 1; they are the Galilei and Morton numbers,

$$Ga = \frac{\sqrt{gD^3}}{\nu}, \quad Mo = \frac{gv^4 \rho^3}{\sigma^3}, \quad (2.2a,b)$$

the number  $N_r$  of rods, the radius  $R_c/(D/2)$  of the cylinder on which the rods are arranged and the ratio  $d/D$  of the rod to the tube diameter. In (2.2a,b)  $\nu$  and  $\rho$  are the liquid

Label	$Ga$	$R_c/\frac{1}{2}D$	$N_r$	$d/D$	$\alpha_s$	$V_{gas}/\frac{\pi}{6}D^3$	$Fr$
A	657	0.70	24	0.067	0.73	1.66	0.56
B	657	0.70	48	0.025	0.55	1.19	0.55
C	657	0.70	24	0.067	0.73	1.19	0.51
D	657	0.70	24	0.067	0.73	1.19	0.50
E	657	0.70	24	0.067	0.73	0.71	0.46
F	625	0.72	24	0.069	0.73	1.84	0.45
G	577	0.76	24	0.073	0.73	2.16	0.36
H	657	0.70	24	0.067	0.73	2.14	—
I	828	0.57	24	0.029	0.38	0.60	—
J	657	0.70	24	0.067	0.73	0.60	0.48
K	828	0.71	8	—	0.33	1.03	0.31
L	828	0.71	16	—	0.33	1.03	0.30

Table 1. Parameter values for the cases shown in this paper; for all simulations,  $Mo = 2 \times 10^{-6}$ . For cases *H* (figure 7*a*) and *I* (figure 8), the gas eventually gets out of the cage and the rise velocity fails to stabilize. Case *J* is for a bubble in the annular space outside the cage, as shown in figure 9(*a*). Cases *K* and *L* are for grooved tubes as shown in figure 9(*b*).

kinematic viscosity and density, and  $\sigma$  is the surface tension coefficient. The fraction of area blocked by the rods, which may be called the solidity of the cage, is  $\alpha_s = N_r d / (2\pi R_c)$ . Our choice of parameters is strongly influenced by computational considerations and may not reflect cases of greater practical relevance in which  $Ga$  would be larger and  $d/D$  and, especially,  $Mo$ , would be significantly smaller. While we have included in the supplementary material available at <https://doi.org/10.1017/jfm.2021.432> the results of some preliminary simulations for  $Mo = 2.5 \times 10^{-11}$ , a value close to that of water, it appears that such situations would be most efficiently studied in a laboratory rather than numerically.

We have found that the fluid mechanics of our system differs in a non-trivial way from that of the standard Taylor bubble case. In order to illustrate the differences and gain some understanding of the present results it is useful to look at the velocity and pressure fields. In describing some typical results, we focus on case *A*, for which the non-dimensional bubble volume is  $V_{gas}/((\pi/6)D^3) = 1.66$  and the bubble length is  $H/D = 2.75$  or  $H/2R_c = 3.93$ . With these values the Froude number of the correlation of Viana *et al.* (2003) is 0.335. Our simulation for an empty tube gave  $U_B/\sqrt{gD} = 0.328$  with a difference of 2.1%. The bubble rise velocity with the cage in place is  $U_B/\sqrt{gD} = 0.56$ , nearly 70% greater than in the empty tube. The shape of the bubble for this case is shown in figure 1(*a*); horizontal views of the tube cross-section from above and from below the bubble can be seen in panels (*b*) and (*c*). The gas penetrates somewhat into the gaps between the rods in the upper part of the bubble (panel *b*), but the extent of these protrusions decreases with depth until the bubble becomes nearly circular toward the bottom (panel *c*).

Figure 3 shows profiles of the flow fields along three horizontal rays passing through the middle of the gap between adjacent rods and extending from the axis at  $r = 0$  to the inner surface of the tube at  $2r/D = 1$ ; the shaded area indicates the radial extent occupied by the rods. The vertical positions at which these results are taken are indicated by the three small black arrows along the tube in figure 4(*c*). From left to right, the three panels show the normalized pressure, horizontal (radial) liquid velocity  $u_r$  and vertical (axial) liquid velocity  $u_z$ , negative downward. The solid lines are for the uppermost ray at the level of the bubble tip; the dashed lines are for a slightly lower ray, at the level at which the bubble

### Faster Taylor bubbles

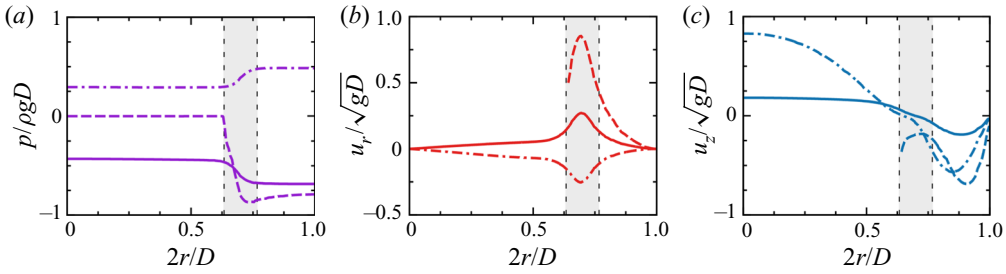


Figure 3. Normalized pressure (a), horizontal velocity (b) and vertical velocity (c) along horizontal rays from the tube axis,  $r = 0$ , to its inner surface,  $r = D/2$ . The solid lines are at a level slightly above the bubble tip, the dashed lines at the base of the cap at the bubble top and the dash-dotted lines slightly below the bubble bottom. These levels are indicated by the small black arrows on the left of figure 4(c).

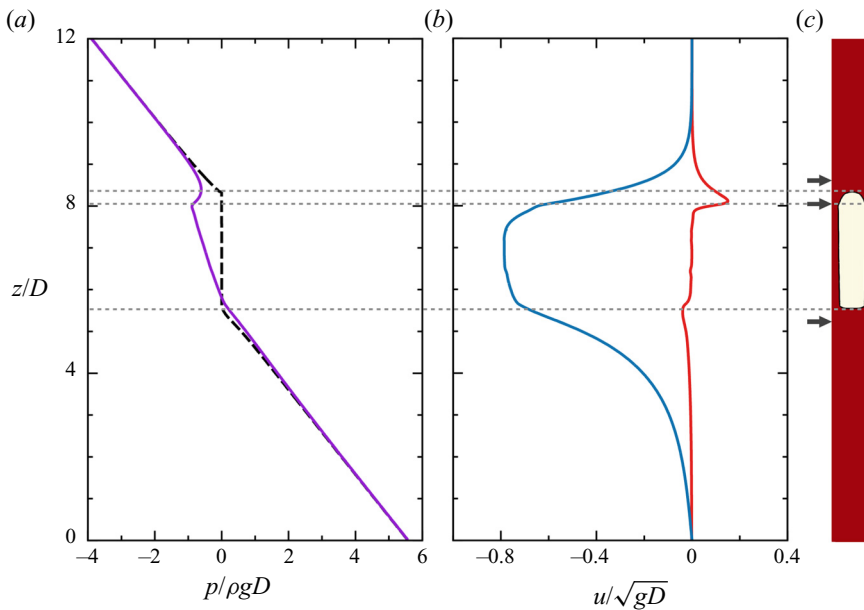


Figure 4. Normalized pressure (solid line in a), horizontal velocity (red line in b) and vertical velocity (blue line in b) along vertical lines corresponding to the midpoint of the gap between adjacent rods and the midpoint of the annulus between the tube wall and the circle of rods. The dashed line in panel (a) is the pressure along the tube axis, which is constant inside the bubble. The small black arrows at the left of panel (c) show the levels at which the radial profiles shown in the previous figures are taken.

cap has expanded to occupy the available core space inside the cage; and the dash-dotted line is at a level slightly below the bubble bottom. The velocity data for the intermediate level start at the bubble surface, since the rest of the cross-section data is occupied by the gas. For the ray at this level the horizontal portion of the pressure line in the core is actually the constant gas pressure inside the bubble.

The pressure at the two upper levels is essentially constant in the core and greater than in the surrounding annulus, with the pressure gradient pushing the liquid out of the core to allow the bubble to rise. The situation is reversed under the bubble, where liquid must flow from the annulus into the core to claim the space vacated by the bubble. The radial velocity,

figure 3(b), is largest (in modulus) at the narrowest point of the gap between rods and is particularly large at the intermediate level where the bubble has first expanded to its largest diameter. The vertical velocity, figure 3(c), is positive above the bubble, although it is significantly lower than the bubble rise velocity. In this region the liquid is pushed laterally into the annulus through the rod cage rather than upward. The vertical velocity is also positive under the bubble, and larger than the rise velocity of the latter. This circumstance indicates the presence of a recirculating wake in the bubble rest frame. At the intermediate level this velocity component is very small in the gap, owing to the no-slip condition at the rod surfaces. In the annulus, it resembles a downward channel-flow behaviour with a small degree of slip at the edge of the rod region.

Corresponding results for pressure and velocity along vertical lines are shown in figures 4(a) and 4(b), respectively. The horizontal thin dashed lines mark significant levels along the bubble, namely the location of the bubble tip, the location where the bubble cap has grown to occupy the tube core and the location of the bubble bottom. The small black arrows along the tube on the left identify the positions at which the radial profiles shown in the previous figure are taken.

The dashed line in figure 4(a) is the pressure along the axis of the tube, which is constant inside the bubble. The other results in panels (a) and (b) are all taken along a vertical line at the middle of the annular region between the rods and the tube wall. Near the top of the bubble the pressure in the annulus is significantly lower than in the core region, as already shown in figure 3. This pressure difference actually markedly and rapidly increases as the cross-section occupied by the bubble reaches its maximum. The core–annulus pressure difference appears localized in a relatively short region above the bubble, while it is smaller and extends downward much farther under the bubble.

The slope of the pressure distribution in the annulus is essentially hydrostatic far ahead of, and far behind, the bubble. However, over much of the bubble length, the pressure gradient is nearly constant and less steep than hydrostatic, indicating the presence of an adverse pressure gradient in the annulus. A clear indication of this effect (which is in marked contrast with the standard Taylor bubble case, for which the pressure in the annulus is essentially constant) is that the gas tends to invade the gaps between the rods more at the top than at the bottom of the bubble, as can be seen in figure 1(b,c). This indicates a pressure increase with depth. The origin of this feature must be sought in the opposite liquid flows out of the tube core near the tip of the bubble and back into the core under it. Since the core pressure just above and just below the bubble is nearly the same (see the black dashed line in figure 4a), these opposite flows require the pressure in the annular region to increase with depth. That this is the correct explanation is supported by our simulations with a thinner annulus (cases *F* and *G*). In these cases the bubble rise velocity is just a little bit larger than for an empty tube, so that the horizontal flow out of and into the cage is reduced. As a consequence, the pressure difference necessary to drive this flow is also smaller and the corresponding adverse pressure gradient less pronounced. This observation suggests that, by reducing the pressure drop across it, a cage made of thin rods or wires could significantly reduce the pressure gradient in the annulus, thus improving the ability of surface tension to confine the gas inside the cage. It may well be worth pursuing this possibility experimentally, because a smaller adverse pressure gradient would enable much longer bubbles to remain contained within the cage.

The blue (left) and red lines in figure 4(b) are the vertical and horizontal velocities. The latter vanishes far above the bubble, then rapidly grows, reaching a sharp maximum in the short length in which the bubble cross-section increases. Behind the bubble the behaviour is more gradual, with the radial velocity small and negative, as will be

### Faster Taylor bubbles

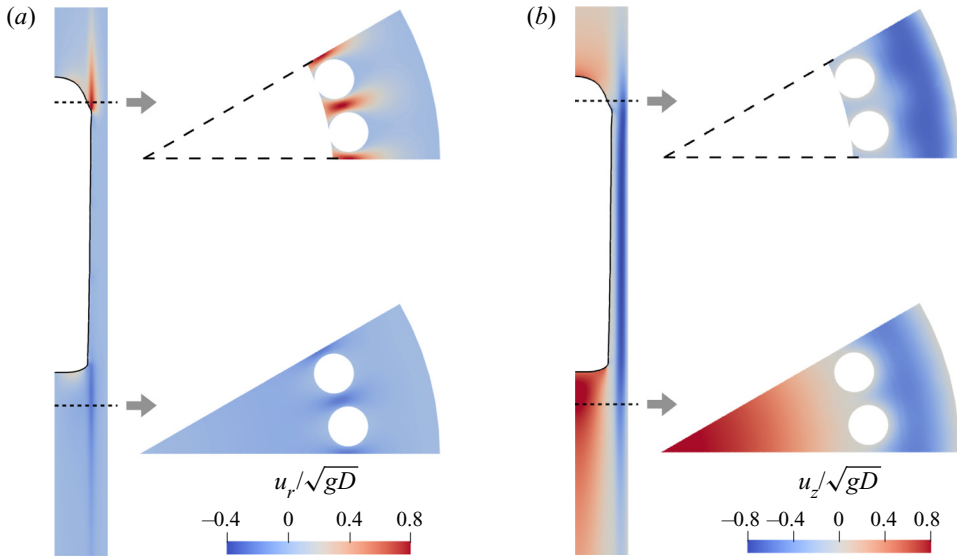


Figure 5. Horizontal (a) and vertical (b) velocity distributions along the tube and on horizontal sectors near the top and bottom of the bubble.

seen more clearly later. The vertical velocity increases significantly in the annulus as the bubble is approached from above, remains fairly large and negative along most of the tube section occupied by the bubble, and then slowly decreases back to zero. The comparison with the nearly vanishing horizontal velocity over much of the tube highlights the quasi-fully-developed channel-like behaviour of the flow through a large portion of the annulus, to which we return below.

A different perspective on the velocity fields is offered by figure 5, which shows, in panels (a) and (b), the radial and axial velocity distributions in vertical cuts of the tube and in two horizontal sectors, one near the top and one just below the bottom of the bubble. The horizontal velocity is quite large in the region above the bubble, becoming nearly jet-like in the gap between the rods and quickly dissipating in the annular region beyond. Under the bubble, the radial velocity is mostly negative as liquid is drawn into the core. The vertical velocity, in panel (b), is negative in the annulus both at the top and under the bubble as liquid is drawn down and into the core, and is large and positive in the core as already seen in figure 3(c). The negative vertical velocity persists for a long distance under the bubble and a shorter one above, giving yet another indication of the difference between the two regions (see also figure 4).

### 3. Theoretical considerations

The constancy of the pressure gradient in the annular space along the bubble shown in figure 4 suggests that the flow in this region can be approximated as fully-developed, an impression strengthened by the near vanishing of the horizontal velocity and the shape of the vertical velocity distribution.

The tube wall imposes a no-slip condition, while, on average, the condition on the circle bounding the cage may be approximated as a partial slip in the form

$$u_z(r = R_c) = s \left. \frac{\partial u_z}{\partial r} \right|_{r=R_c}, \quad (3.1)$$

with  $s$  a suitable slip length and the  $z$  axis, coincident with the tube axis, positive upward. The pertinent form of the Navier–Stokes equations in the axial direction is readily solved (see e.g. Goldsmith & Mason 1962), and the following expression for the liquid flow rate is obtained after imposing the appropriate boundary conditions:

$$Q = -\pi \frac{\rho g + \partial_z p}{8\mu} \left[ (R_t^2 - R_c^2)^2 - \frac{R_t^2 - R_c^2 + 2sR_c}{\log(R_t/R_c) + s/R_c} \left[ R_t^2 - R_c^2 - 2R_c^2 \log(R_t/R_c) \right] \right], \tag{3.2}$$

with  $R_t = D/2$  the tube radius. By conservation of volume,  $Q$  must balance the rate at which the bubble, rising with velocity  $U_B$ , makes room available under its base, approximately given by  $\pi R_c^2 U_B$ , so that  $\pi R_c^2 U_B = -Q$ .

Equation (3.2) is appropriate along the body of the bubble, where there is little if any exchange of liquid between the inside and outside of the cage, so that  $Q$  is essentially constant. However, the flow rate through the annulus in the regions above and below the bubble cannot be constant, as liquid must be pushed out of the cage by the rising top and pulled back into the cage by the rising bottom. As already noted, these processes require suitable pressure gradients in the horizontal direction which we have seen earlier in figure 3(a). If we approximate the flow in the gap between the rods as a Poiseuille flow in a two-dimensional channel with an effective width  $h_{eff}$ , we can estimate the local flow rate per unit height through each gap as

$$q = \frac{h_{eff}^3}{12\mu} \frac{p_{in}(z) - p(z)}{d}, \tag{3.3}$$

where  $p_{in}(z)$  and  $p(z)$  are the pressures inside and outside the cage; the fraction in this equation approximates the pressure drop across the rod cage. This flow affects the flow rate in the annulus,  $dQ/dz = N_r q$ . By making a quasi-equilibrium approximation, we use (3.2) for  $Q$  in this equation, finding

$$\frac{\partial^2 p}{\partial z^2} - \ell^{-2} p = -\ell^{-2} p_{in}(z). \tag{3.4}$$

This relation identifies the characteristic length scale for the effect of the flow into and out of the cage as

$$\ell = \sqrt{\frac{3\pi d}{2N_r h_{eff}^3} \left[ R_t^4 - R_c^4 - \frac{(R_t^2 - R_c^2)^2}{\log(R_t/R_c)} \right]}. \tag{3.5}$$

The slip length can be estimated to be very small in our case and has been neglected here. By approximating the pressure inside the cage above the bubble as hydrostatic on the basis of figure 4 and other results (not shown), the solution of (3.4) decreasing far upstream is readily found to be

$$p(z) = p_{in}(z) + [p(z_t) - p_{in}(z_t)] \exp(-(z - z_t)/\ell), \tag{3.6}$$

with  $p_{in}(z) = p_{in}(z_t) - \rho g(z - z_t)$ ,  $z_t$  corresponding to the highest point of the bubble top. The difference  $\Delta p = p - p_{in}$  is indeed exponential for a significant distance above the bubble, as shown in figure 6(a). The characteristic length of the exponential in this case is found to be  $\ell/D = 0.4$ , and it becomes equal to the value in (3.5) upon taking the effective gap width  $h_{eff}/h \simeq 2.16$ , with  $h$  the minimum width of the inter-rod gap. Application of (3.4) to the region under the bubble is more difficult, because the behaviour of the pressure

## Faster Taylor bubbles

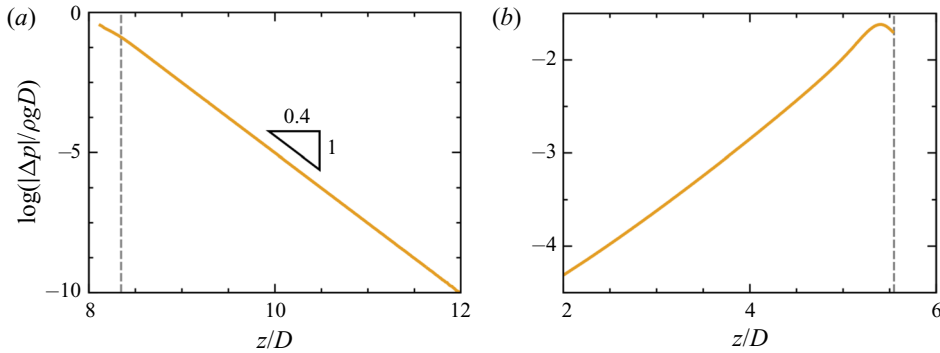


Figure 6. Logarithm of the normalized core–annulus pressure difference, above (a) and below (b) the bubble, as a function of vertical position. The vertical dashed lines mark the position of the bubble top in (a) and of the bubble bottom in (b). The characteristic length of the exponential in (3.6) has the value  $\ell/D = 0.4$ . In (a), the portion of the line to the left of the dashed line is the region of the bubble top.

in the core region cannot be approximated as simply as above, as is evident from figures 4 and 6(b).

Consideration of the results presented thus far also permits us to draw some general conclusions on the effects of the bubble length and of the annulus thickness. Concerning the former, suppose that the rise velocity and the adverse pressure gradient in the annulus were to remain the same as the bubble length is increased. This would create a bigger inner–outer pressure difference at the top and/or bottom of the bubble, increasing the flow out of and/or into the annulus. This effect would make it impossible for the rise velocity to remain unchanged. Suppose then that the rise velocity were to remain constant with the adverse pressure gradient in the annulus becoming smaller. This would result in a bigger downward flow rate as the effect of gravity becomes less hindered, which again would be incompatible with the assumption of a constant rise velocity. If the rise velocity of a longer bubble were smaller than that of a shorter one, this would require a stronger adverse pressure gradient, causing a bigger pressure difference at the top and/or bottom of the bubble, which, again, would require a faster rise velocity. Thus, unlike the standard Taylor bubble case, as the bubble length increases, so does its rise velocity. This increased velocity must be compensated by a greater downward flow in the annulus, which, in turn, requires a weaker adverse pressure gradient. Thus it may be concluded that longer bubbles rise faster with a weaker adverse pressure gradient in the annulus.

Consider now the effect of the thickness of the annulus. If the adverse pressure gradient were to remain the same as the thickness is increased, the downward liquid flow rate would increase and, with it, so would the bubble rise velocity. But the flow into and out of the cage, which determines the rise velocity, is little affected by the annulus thickness, which would be incompatible with an increase in velocity. Thus, it must be concluded that increasing the annulus thickness increases the adverse pressure gradient and the bubble rise velocity. We will see a confirmation of these expectations in the next section.

### 4. Some additional results

The acceleration of the rise velocity of a Taylor bubble described in this work depends on too many parameters to permit an exhaustive investigation. Nevertheless it is interesting to look at some other results that give some indication of what might be expected with other parameter values.

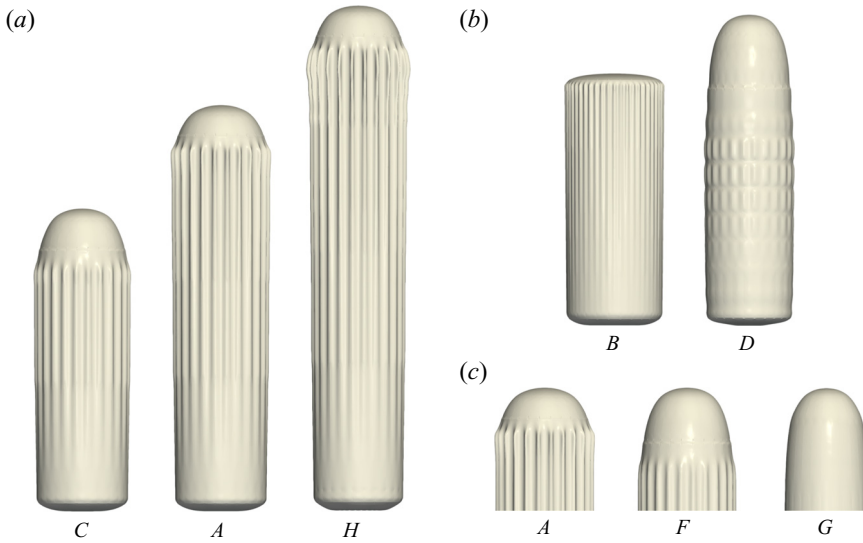


Figure 7. Some additional examples of computed bubble shapes; the letters labelling each image correspond to those labelling the Froude numbers in figure 2 and to the cases in table 1. The middle bubble in (a) is the same as that shown in figure 1; the two bubbles flanking it differ only in the amount of gas they contain. The left bubble in panel (b) rises in a cage with a larger number of thinner rods and a larger porosity. For the right bubble in (b) the vertical rods of the cage are connected by evenly spaced collars with the same diameter as the vertical rods. The second and third bubbles in panel (c) rise in tubes with diameters 3.3% and 8.3% smaller than that of the first bubble.

Figure 7 shows different computed bubble shapes for several cases. The middle image in panel (a) is the same as that shown in figure 1. The images flanking it differ only in the gas volume and, therefore, the bubble length. In agreement with the considerations at the end of the previous section, the shorter bubble C rises more slowly than the longer bubble A. A steady rise velocity for the longest bubble H is actually not reached, because, while it is still growing beyond the velocity of bubble A, at some point the gas breaks out of the cage. This confirms the earlier statement (§ 2) about the possibility that the pressure gradient in the annulus could limit the length of bubbles that can be contained for a given surface tension. It can indeed be seen in panel (a) how, at the top of the bubbles, the gas increasingly penetrates the gap between the rods as the bubble length increases.

An example of what might happen when containment fails is shown in figure 8 (case I), in which the gas has formed ‘belts’ outside the cage enveloping the rods, and the rise velocity does not stabilize. The same eventually happens for the longest bubble of figure 7(a). The left bubble in figure 7(b) is for case B, in which the cage has a larger porosity. In this case the characteristic length  $\ell$  defined in (3.5) is smaller than in case A, which implies a stronger axial pressure gradient, which pushes on the bubble top, increasing its radius of curvature. The right bubble in figure 7(b) rises in a cage in which evenly spaced horizontal circular collars, or hoops, connect the rods. In this case, the presence of two, rather than one, finite radii of curvature helps surface tension contain the bubble, and, indeed, the figure shows that the gas pushes out of the cage less than in the cases of panel (a). The influence of the annulus thickness is shown in figure 7(c), in which the first bubble is the same as in figure 1 while the other two are for annuli thinner by 11.1% and 27.8% (corresponding to tube diameters smaller by 3.3% and 8.3%) with the same cage radius. As discussed in § 2, in these cases the pressure difference in the

Faster Taylor bubbles

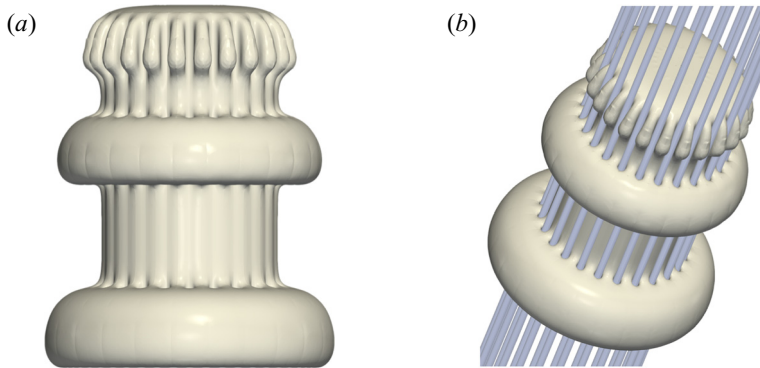


Figure 8. Two views of the bubble of case *I*, for which surface tension is unable to contain the gas within the rod cage; in this case the rise velocity does not stabilize.

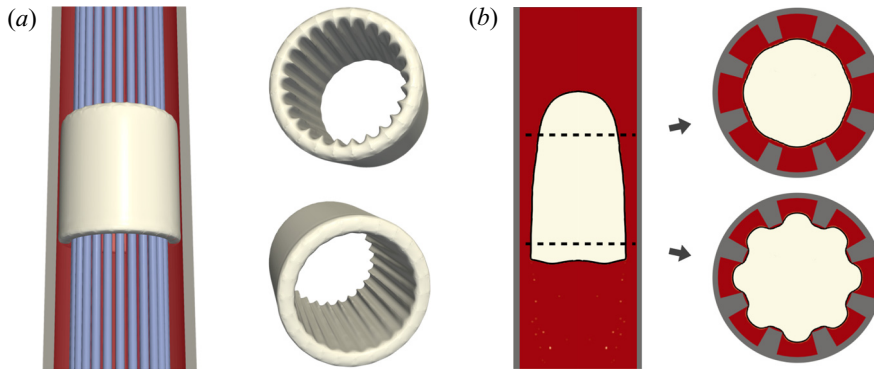


Figure 9. Two alternative implementations of the principle described in this paper. (a) An arrangement in which the bubble is outside the cage, occupying the annular space between the cage and the tube wall (case *J*). This configuration is also successful in increasing the rise velocity, as shown in [figure 2](#) and [table 1](#). (b) The case *K* bubble rising in a tube with grooves etched in the tube wall to help promote the downward flow of liquid.

annulus between the top and bottom of the bubble is smaller because of the reduced rise velocity, and the gas protrudes significantly less into the gap between the rods.

[Figure 9\(a\)](#) shows another possible implementation of the present idea (case *J*). Here the gas is confined within the annular space between the cage of rods and the tube wall. As can be seen in [figure 2](#), the resulting increase in the bubble rise velocity is quite significant in spite of the relatively small gas volume. Yet another possible implementation is shown in [figure 9\(b\)](#), in which the downward flow of liquid along the bubble occurs in grooves etched along the wall. With the parameters used for these simulations (cases *K* and *L* in [table 1](#)), the Reynolds number for the groove flow is relatively small, and the liquid flow is too slow to result in an increase of the rise velocity. In these cases the rise velocity is actually somewhat smaller than the value predicted by the correlation of Viana *et al.* (2003) for a round tube having the same (outer) diameter.

## 5. Numerical aspects

The three-dimensional numerical simulations were carried out by using the volume-of-fluid Navier–Stokes solver *interIsoFoam* embedded in the open-source software *OpenFOAM* v2012. This solver is designed for two incompressible, isothermal immiscible fluids with the surface tension force between phases modelled as a continuum surface force (CSF; Brackbill, Kothe & Zemach 1992). The *isoAdvector* phase-fraction-based interface-capturing approach (Roenby, Bredmose & Jasak 2016) is used to enhance the sharpness of the gas–liquid interface. The flow fields were updated in time with the second-order backward scheme, while the upwind-biased second-order scheme was used for the advection term. The phase fraction field was updated with the Crank–Nicolson method, and the van Leer limiter was used for the advection term.

In most cases, a sector of the tube containing only one rod was simulated with symmetry boundary conditions along the radial surfaces and a no-slip condition on the solid surfaces. The rod was assumed to be fully wetted with a zero solid–liquid contact angle. The simulated tube had a length of  $L/D \simeq 12$  or larger with its top and bottom ends closed (no-slip condition). The bubble was released near the bottom and evolved to a steady shape and constant rise velocity which began to be affected by the domain top only when the bubble was in close proximity to it. All the data reported in the paper were taken well before this time. We set both the density and the kinematic viscosity of the gas to be 1000 times smaller than those of the liquid. On the basis of previous experience with related problems we are confident that the gas flow had a negligible effect on the phenomenon simulated. The pressure in the bubble was taken as the reference pressure.

The typical mesh consisted of about 4.8 million cells and was refined in the vicinity of the rod in order to resolve the flow in the gap between the rods. For our base case *A* we also used a coarser mesh with 1.0 million cells, finding a difference of only 1.1 % in the calculated Froude number. Nevertheless, we used the finer mesh for the data shown in the figures. As mentioned in § 2, we also simulated the rise of the bubble in an empty tube (i.e. without the cage) with comparable cell size and distribution; here we found good agreement with the correlation from the literature, which was built on an extensive data bank.

## 6. Conclusions

A principle that can be used to increase the rise velocity of Taylor bubbles in tubes by artificially enlarging the space available for the liquid downflow is described in this paper. While we have focused on bubble rise by buoyancy, the same principle may be expected to be applicable to pressure-driven Taylor-bubble flow. Applications of this idea may be found in flow boiling (particularly with the arrangement of figure 9(a), since the vapour is produced at the tube wall), in which fast vapour removal may be desirable both to increase the rate at which vapour is supplied to turbines and to diminish the danger of burn-out. Other applications may be found in the removal of gaseous products of liquid-phase chemical reactions, microfluidics and others. Of course the rise velocity of Taylor bubbles can be increased by using larger tubes, but this option incurs a greater cost and requires more space. Possibly because this arrangement opens up a wider passage for the film flow, the rise velocity can also be increased by inclining the tube (see e.g. Alves, Shoham & Taitel 1993; de Azevedo, Faccini & Su 2020), but, again, this would increase the footprint of the installation.

The verification of this principle in a laboratory appears to present little difficulty and may be more appropriate than computation, which is limited in its ability to deal with

thin rods, large Reynolds numbers and complex geometries. While we have demonstrated a speed-up of nearly 70 % with respect to a standard Taylor bubble, it is quite possible that this result does not represent an upper limit. Experiments would permit the identification of optimal conditions and an exhaustive exploration of the parameter space. In an experiment it may be convenient to construct the cage as a net, rather than an array of rods, as the presence of a finite curvature in the second direction would assist surface tension in confining the gas inside the cage, as noted above.

Numerous variants of the basic principle described here are possible, such as vertical grooves etched in the tube wall. Our limited exploration of this option for cases *K* and *L* (figure 9*b*) has not proven very promising, but this could be due to the relatively low Reynolds number that we considered to simplify the numerical work. Of course, implementation of the idea in this way would require a thicker, and therefore heavier and costlier, tube. Use of a cage to limit the horizontal spread of the gas may also be useful in the case of so-called spherical cap bubbles in an unconfined liquid, the rise velocity of which is limited by the increasing drag that they encounter as their frontal area increases with the volume of gas that they enclose.

**Supplementary material.** Supplementary material is available at <https://doi.org/10.1017/jfm.2021.432>.

**Acknowledgements.** The numerical computations were carried out on the Sabine cluster of the University of Houston Research Computing Data Core.

**Funding.** Research reported in this paper was supported by the Gulf Research Program of the National Academies of Sciences, Engineering, and Medicine under award number GRP2000008864. The content is solely the responsibility of the authors and does not necessarily represent the official views of the Gulf Research Program or the National Academies of Sciences, Engineering, and Medicine.

**Declaration of Interests.** The authors report no conflict of interest.

#### Author ORCIDs.

 Andrea Prosperetti <https://orcid.org/0000-0003-4129-7130>.

#### REFERENCES

- ALVES, I.N., SHOHAM, O. & TAITEL, Y. 1993 Drift velocity of elongated bubbles in inclined pipes. *Chem. Engng Sci.* **48**, 3063–3070.
- DE AZEVEDO, M.B., FACCINI, J.L.H. & SU, J. 2020 Experimental study of single Taylor bubbles rising in vertical and slightly deviated circular tubes. *Exp. Therm. Fluid Sci.* **116**, 110109.
- BARNEA, D. 1990 Effect of bubble shape on pressure drop calculations in vertical slug flow. *Intl J. Multiphase Flow* **16**, 79–89.
- DEL BELLO, E., LLEWELLIN, E.W., TADDEUCCI, J., SCARLATO, P. & LANE, S.J. 2012 An analytical model for gas overpressure in slug-driven explosions: insights into strombolian volcanic eruptions. *J. Geophys. Res.* **117**, B02206.
- BENDIKSEN, K.H. 1985 On the motion of long bubbles in vertical tubes. *Intl J. Multiphase Flow* **11**, 797–812.
- BI, Q.C. & ZHAO, T.S. 2001 Taylor bubbles in miniaturized circular and noncircular channels. *Intl J. Multiphase Flow* **27**, 561–570.
- BRACKBILL, J.U., KOTHE, D.B. & ZEMACH, C. 1992 A continuum method for modeling surface tension. *J. Comput. Phys.* **100**, 335–354.
- BREHERTON, F.P. 1961 The motion of long bubbles in tubes. *J. Fluid Mech.* **10**, 166–188.
- CLANET, C., HÉRAUD, P. & SEARBY, G. 2004 On the motion of bubbles in vertical tubes of arbitrary cross-sections: some complements to the Dumitrescu–Taylor problem. *J. Fluid Mech.* **519**, 359–376.
- DAVIES, R.M. & TAYLOR, G.I. 1950 The mechanics of large bubbles rising through extended liquids and through liquids in tubes. *Proc. R. Soc. Lond. A* **200**, 375–390.
- DUMITRESCU, D.T. 1943 Strömung an einer Luftblase im senkrechten Rohr. *Z. Angew. Math. Mech.* **23**, 139–149.
- FABRE, J. & LINÉ, A. 1992 Modeling of two-phase slug flow. *Annu. Rev. Fluid Mech.* **24**, 21–46.

- FERNANDES, R.C., SEMIAT, R. & DUKLER, A.E. 1983 Hydrodynamic model for gas-liquid slug flow in vertical tubes. *AIChE J.* **29**, 981–989.
- FUNADA, T., JOSEPH, D.D., MAEHARA, T. & YAMASHITA, S. 2005 Ellipsoidal model of the rise of a Taylor bubble in a round tube. *Intl J. Multiphase Flow* **31**, 473–491.
- GOLDSMITH, H.L. & MASON, S.G. 1962 The movement of single large bubbles in closed vertical tubes. *J. Fluid Mech.* **14**, 42–58.
- GONNERMANN, H.M. & MANGA, M. 2007 The fluid mechanics inside a volcano. *Annu. Rev. Fluid Mech.* **39**, 321–356.
- KAWAGUCHI, R. & NISHIMURA, T. 2015 Numerical investigation of temporal changes in volcanic deformation caused by a gas slug ascent in the conduit. *J. Volcanol. Geotherm. Res.* **302**, 1–10.
- KULKARNI, A.A. & JOSHI, J.B. 2005 Bubble formation and bubble rise velocity in gas-liquid systems: A review. *Ind. Engng Chem. Res.* **44**, 5873–5931.
- LIBERZON, D., SHEMER, L. & BARNEA, D. 2006 Upward-propagating capillary waves on the surface of short Taylor bubbles. *Phys. Fluids* **18**, 048103.
- LIZARRAGA-GARCIA, E., BUONGIORNO, J., AL-SAFRAN, E. & LAKEHAL, D. 2017 A broadly-applicable unified closure relation for Taylor bubble rise velocity in pipes with stagnant liquid. *Intl J. Multiphase Flow* **89**, 345–358.
- LLEWELLIN, E.W., DEL BELLO, E., TADDEUCCI, J., SCARLATO, P. & LANE, S.J. 2012 The thickness of the falling film of liquid around a Taylor bubble. *Proc. R. Soc.* **A468**, 1041–1064.
- MAGNINI, M., KHODAPARAST, S., MATAR, O.K., STONE, H.A. & THOME, J.R. 2019 Dynamics of long gas bubbles rising in a vertical tube in a cocurrent liquid flow. *Phys. Rev. Fluids* **4**, 023601.
- NOGUEIRA, S., RIETHMULER, M.L., CAMPOS, J.B.L.M. & PINTO, A.M.F.R. 2006 Flow in the nose region and annular film around a Taylor bubble rising through vertical columns of stagnant and flowing Newtonian liquids. *Chem. Engng Sci.* **61**, 845–857.
- ROENBY, J., BREDMOSE, H. & JASAK, H. 2016 A computational method for sharp interface advection. *R. Soc. Open Sci.* **3**, 160405.
- VIANA, F., PARDO, R., YÁNEZ, R., TRALLERO, J.L. & JOSEPH, D.D. 2003 Universal correlation for the rise velocity of long gas bubbles in round pipes. *J. Fluid Mech.* **494**, 379–398.
- WALLIS, G.B. 1969 *One-Dimensional Two-Phase Flow*. McGraw-Hill, reprinted by Dover, 2020.
- ZHANG, M.H., PAN, L.M., HE, H., YANG, X.H. & ISHII, M. 2018 Experimental study of vertical cocurrent slug flow in terms of flow regime transition in relatively small diameter tubes. *Intl J. Multiphase Flow* **108**, 140–155.